# The Impact of Non-Isotropic Scattering and Directional Antennas on MIMO Multicarrier Mobile Communication Channels

Hamidreza Saligheh Rad and Saeed Gazor

***Abstract*—In outdoor environments, waves propagate non-isotropically because of non-uniform distribution of scatterers. In addition directional antennas, which are efficient for communication applications, have considerable impact on the response of the communication channel. The impact of non-isotropic propagation and directional antennas is more significant when the system employs multiple antennas. In this paper, we propose a space-time-frequency cross-correlation function (CCF) for multiple-input multiple-output multicarrier channels in a two-dimensional (2D) random scattering medium. The expression of the CCF turns out to be a multiplication of three CCFs. Two of these terms characterize the impact of mobile station and base station, respectively and are linear Bessel expansions, where the coefficients are given by the linear convolution of the Fourier series coefficients (FSC)s of the employed antenna patterns and the FSCs of the probability density function describing 2D non-isotropic environment. The third expression characterizes the impact of the wireless channel. In the stationary case, we derive the expression of the fading channel power spectrum (CPS) in terms of the non-isotropic pdf and antenna patterns. Using the expression of the CCF, we also calculate coherence-bandwidth (CB)/coherence-time (CT) as a function of carrier-frequency/time separations. Our numerical results show a good fit to the available experimental results obtained for the CB/CT of realistic outdoor channels.**

***Index Terms*—MIMO wireless channel, space-time-frequency cross-correlation function, random scattering media, non-isotropic propagation channel, directional antennas, coherence-time, coherence-bandwidth and power spectral density.**

## I. Introduction

Wireless communication channels are significantly influenced by non-uniform distribution of scatterers in the space as well as by the directional antenna propagation patterns (APP), (i.e., by APP we mean the response of the antenna to different directions in space). Accurate small-scale fading models of these channels play a significant role to achieve the full potential capacity of multiple-input multiple-output (MIMO) multicarrier mobile communication systems. The small-scale fading is considered due to the small movements of the mobile station (MS) as well as different characteristics of the multipath propagation medium which results in fluctuations in the received power level [1]. More precisely, this fading behavior highly depends on the distribution of scatterers in the space, the antenna propagation patterns (APP)s, and the direction and the speed of the MS.

A comprehensive approach to characterize MIMO channels is to analyze the statistical behavior of the space-time-frequency (STF) channel transfer function (CTF) in terms of different characteristics of the propagation environment and the communication system [2]–[5]. In this approach, the CTF is represented by a sum of propagation waveforms over a number of paths. In each path, the signal reaches the receiver with a response described by the probability density functions (pdf)s of some random variables. These random variables are phase, delay, direction-of-departure (DOD), and direction-of-arrival (DOA). In order to describe a non-isotropic propagation medium, most of existing MIMO channel models assume either a function for the energy distribution of the propagating waveforms versus directions or a pdf for the propagating directions. Such an energy distribution is often called power azimuth spectrum (PAS), while such a pdf for propagating directions is known as azimuth angular spread (AAS). In the literature, these distributions are justified using experimental results [6]–[10]. Martin in [6] suggests a Laplacian (double-sided exponential) pdf for the relative DOA of the first multipath component, i.e., for the line-of-sight (LOS), and a zero-mean truncated Normal pdf for the relative DOA variables associated with other paths. Pedersen, Mogensen, and Fleury find that in typical urban environments, PAS is accurately described by a Laplacian function, while a Gaussian function matches the shape of the AAS [7]. Abdi, Barger, and Kaveh propose the use of the versatile von-Mises angular distribution for modeling the nonuniform AAS at the MS [8]. This distribution accurately approximates relevant distributions such as uniform, impulse, cardioid, Gaussian, and wrapped Gaussian. Zekavat and Nassar in [9] introduce the secant-square PAS model as a simple mathematical model and a better fit to real measured data to the TSUNAMI II project [7]. Finally, Ao and Ke in [10] show that the PAS in microcellular environments can be approximated by a truncated Laplacian distribution, based on the elliptical scattering model.

In [5], an STF model is proposed for a 2D isotropic propagation environment and employing omnidirectional APPs. By extending this model, we calculate the STF cross-correlation function (CCF) between two sub-channels of a mobile multicarrier MIMO channel versus different antenna elements,

Paper approved by Y. Li, the Editor for Wireless Communication Theory of the IEEE Communications Society. Manuscript received March 12, 2006; revised October 16, 2006.

H. S. Rad is with the Division of Engineering and Applied Sciences, Harvard University, Cambridge, MA (e-mail: hamid@deas.harvard.edu).

S. Gazor is with the Department of Electrical and Computer Engineering, Queen's University, Kingston, Ontario K7L 3N6, Canada (e-mail: s.gazors@queensu.ca).

Digital Object Identifier 10.1109/TCOMM.2008.060121.

time-indices, and carrier frequencies. We represent the non-isotropic scatterers by the Fourier series expansion (FSE) of the pdf of the propagating directions. We also consider the effect of the directional antenna element patterns by the FSE of the APPs. The expression of the CCF turns out to be a composition of linear expansions of Bessel functions of the first kind. The CCF shows different impacts of non-isotropic wave propagation, directional antennas, and the direction of MS motion on the shape of the channel power spectrum. Since the existing experimental results reveal that the third dimension of the space can have noticeable effects on the CCF, the investigation on the impacts of the elevation angle is still an active research subject in wireless channel modeling [11]–[14].

The rest of this paper is organized as follows: Notations and assumptions are introduced in Section II. In Section III, the proposed CCF is derived and analyzed considering the impact of non-uniform AASs and directional antennas. Coherence time and coherence bandwidth are calculated in Section IV-C. Conclusions are summarized in Section V.

## II. MIMO Non-Isotropic Propagation Channel

In this section, we introduce employed notations and assumptions for a MIMO wireless channel in a 2-dimensional (2D) non-isotropic random scattering medium along with directional antenna arrays. Throughout this paper superscripts $B$ and $M$ indicate variables at the BS and the MS sides, respectively. Consider a moving MS with a constant speed vector $\mathbf{v}(\frac{\mathrm{m}}{\mathrm{sec}})$ and a fixed BS. Antenna elements are located on the 2D azimuthal plane at MS and BS sides around their local coordinates, $O^B$ and $O^M$. We assume a propagation pattern for each antenna element denoted by $G_p^B(\Theta^B;\omega)$ and $G_m^M(\Theta^M;\omega)$ at frequency $\omega$, for the $p^{\text{th}}$ antenna at the BS and the $m^{\text{th}}$ antenna at the MS, respectively, where $\Theta^B \triangleq \angle\mathbf{\Theta}^B$ and $\Theta^M \triangleq \angle\mathbf{\Theta}^M$. The unity vectors $\mathbf{\Theta}^B$ or $\mathbf{\Theta}^M$ represent a propagation direction (DOD or DOA) at BS or MS, respectively. Antenna elements are addressed by position vectors $\mathbf{a}_p^B$ and $\mathbf{a}_m^M$ versus local coordinates. We assume that the distance between scatterers and antenna arrays is much larger than the inter-element antenna distances, therefore, propagation waveforms in the scattering environment are plane waves and there is no inter-element scattering. We also assume that the number of propagation paths is large enough such that the channel is Rayleigh by virtue of the central limit theorem. In other words, we assume multipath propagation with no line-of-sight; however, the line-of-sight propagation path between the transmitter and the receiver can be separately treated [4].

In the multipath propagation environment, the received signal is composed of a linear combination of plane waves where each received waveform (the $i^{\text{th}}$ received waveform) is associated with a attenuation gain $g_{p,m;i}$, a path phase shift $\phi_i$, a time-varying delay $\tau_{p,m;i}(t)$, and an antenna gain composed of the pattern elements at both BS and MS $G_p^B(\Theta_i^B;\omega)G_m^M(\Theta_i^M;\omega)$, where $\Theta_i^B$ and $\Theta_i^M$ are propagation directions associated with $i^{\text{th}}$ path. The APPs $G_p^B(\Theta^B;\omega)$ and $G_m^M(\Theta^M;\omega)$ are deterministic functions in terms of the propagation direction and the frequency. The CTF between the BS antenna located at $\mathbf{a}_p^B$ and the MS antenna located at $\mathbf{a}_m^M$ is represented in terms of the carrier frequency as shown in (1), where $I$ is the number of dominant paths resulting from scattering, the Doppler shift $\frac{\omega}{c}\mathbf{v}^T\mathbf{\Theta}_i^M$ denotes the frequency shift of the signal along $i^{\text{th}}$ path caused by the Doppler effect, $\omega$ is the carrier frequency, and $\mathbf{v}$ and $c$ are the MS velocity vector and the speed of light, respectively. The CTF, $h_{pm}(t,\omega)$, is the gain between baseband representation of the input and the output of the channel assuming a narrowband transmitted signal. A signal is defined narrowband in comparison with the channel if the channel response, $h_{pm}(t,\omega)$ is almost constant within the frequency range $\omega \in [\omega_0 - W, \omega_0 + W]$, where $[\omega_0 - W, \omega_0 + W]$ is the signal bandwidth around the carrier frequency $\omega_0$. From (1) we note that the CTF must be a function of the statistics of all DODs and DOAs. The propagation delay over $i^{\text{th}}$ path, $\tau_{p,m;i}(t) \triangleq \tau_{p,m;i} + \frac{t}{c}\mathbf{v}^T\mathbf{\Theta}_i^M$, is time-varying due to the mobility of the MS. We also make the following assumptions:

A1) The pdf of the propagation directions, $f^B(\Theta^B)$ and $f^M(\Theta^M)$ over $[-\pi,\pi)$, characterize the non-isotropic propagation environment around the BS and the MS, respectively. Since these pdfs are periodic with period $2\pi$, we can represent them by their FSE pairs as follows:

$$\mathcal{F}_k^B \longleftrightarrow f^B(\Theta^B) \text{ and } \mathcal{F}_k^M \longleftrightarrow f^M(\Theta^M), \tag{2a}$$

$$\mathcal{F}_k = \frac{1}{2\pi}\int_{-\pi}^{\pi} f(\Theta)e^{-jk\Theta}d\Theta \text{ and } f(\Theta) = \sum_{k=-\infty}^{+\infty}\mathcal{F}_k e^{jk\Theta}. \tag{2b}$$

These pdfs are real and positive functions. If we assume even functions for these angular distributions, then $\mathcal{F}_k^M$ and $\mathcal{F}_k^B$ are also real and even functions versus $k$. Reported measurement results in literature [6]–[10] suggest the following two candidates for the pdf of the non-isotropic AAS $f_{\mathbf{\Theta}}(\Theta)$, (and their corresponding FSCs $\mathcal{F}_k$), namely truncated-Normal and truncated-Laplace distributions ($\forall\Theta \in [-\pi,\pi)$ and $k \in \mathbb{Z}$):

$$\text{Truncated Laplace:}\quad f_{\mathbf{\Theta}}(\Theta) = \frac{\exp\left(-\frac{|\Theta|}{a}\right)}{2a\left(1-e^{-\frac{\pi}{a}}\right)},$$

$$\mathcal{F}_k = \frac{e^{-\frac{\pi}{a}}(-1)^{k+1}+1}{2\pi\left(1-e^{-\frac{\pi}{a}}\right)\left(1+k^2a^2\right)}, \tag{3}$$

$$\text{Truncated Normal:}\quad f_{\mathbf{\Theta}}(\Theta) = \frac{\exp\left(-\frac{\Theta^2}{2a^2}\right)}{\operatorname{erf}\left(\frac{\pi}{\sqrt{2}a}\right)\sqrt{2\pi}a},$$

$$\mathcal{F}_k = \frac{\operatorname{Re}\left\{\operatorname{erf}\left(\frac{\pi+ja^2k}{\sqrt{2}a}\right)\right\}\exp\left(-\frac{k^2a^2}{2}\right)}{\operatorname{erf}\left(\frac{\pi}{\sqrt{2}a}\right)}, \tag{4}$$

$$\text{Aliased -Normal:}\quad f_{\mathbf{\Theta}}(\Theta) = \frac{1}{\sqrt{2\pi}a}\sum_{k=-\infty}^{\infty} e^{-\frac{(\Theta-2\pi k)^2}{2a^2}},$$

$$\mathcal{F}_k = \frac{1}{2\pi}\exp\left(-\frac{a^2k^2}{2}\right). \tag{5}$$

where $\operatorname{Re}(.)$ represents the real part of a complex vari-

$$h_{pm}(t,\omega)=\sum_{i=1}^{I} G_p^B(\Theta_i^B;\omega)G_m^M(\Theta_i^M;\omega)g_{p,m;i}\exp\left(j\phi_i - j\frac{\omega}{c}\mathbf{v}^T\boldsymbol{\Theta}_i^M t - j\omega\tau_{p,m;i}\right) \quad (1)$$

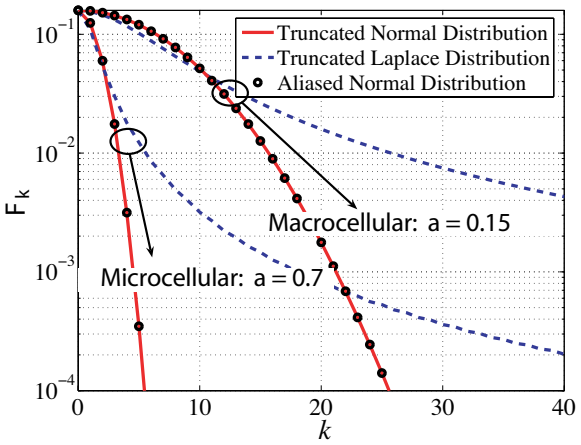


Fig. 1. **Fourier Series Coefficients for different AAS pdfs** to approximate truncated Laplace, truncated Normal and aliased Normal distributions in order to have a good match to the real pdf for different propagation environments; macrocellular ($a = 0.15$rad) and microcellular ($a = 0.7$rad) environments.

able and $\mathrm{erf}(z) \triangleq \frac{2}{\sqrt{\pi}}\int_0^z e^{-\xi^2}d\xi$ is the error function for $z \in \mathbb{C}$. We suggest to use an aliased form of the Normal pdf in order to reduce the computational complexity of the coefficients instead of the truncated Normal pdf. The local distribution of scatters around the MS and BS are different; the environment around the MS is usually considered as a microcellular environment, while the environment around the BS is a macrocellular environment [7]. However, the above pdfs characterize the statistics of the angular dispersions at both BS and MS by using different appropriate values for $a$ (smaller value for the BS side). Figure 1 compares the FSCs of these pdfs for two different macrocellular and microcellular situations; $a = 0.15$rad and $a = 0.70$rad, respectively. For practical values of $a$ ($a < 1$), the aliased Normal pdf is very close to the truncated Normal pdf. We therefor propose to use the aliased Normal pdf because the aliased Normal pdf has simpler expression for FSCs. Let $N_\epsilon$ denote the required number of FSCs in order to approximate the above pdfs with the requires accuracy $\epsilon$, such that $\forall k > N_\epsilon : |\mathcal{F}_k| < \epsilon$. Comparing the distributions in Figure 1, we see that the necessary number of FSCs for the Laplace pdf is $N_\epsilon = \frac{1}{a}\sqrt{\left(\frac{1+e^{-\frac{\pi}{a}}}{1+e^{-\frac{\pi}{a}}}\right)\frac{1}{2\pi\epsilon}-1} \approx \frac{1}{a\sqrt{2\pi\epsilon}}$ larger than the necessary number of FSCs for the Normal pdf $N_\epsilon = \frac{1}{a}\sqrt{-2\ln(2\pi\epsilon)}$.

A2) The complex APPs, $G_p^B(\Theta^B;\omega)$ and $G_m^M(\Theta^M;\omega)$, give the response of the pattern elements in terms of the propagation directions and the carrier frequency. These pattern functions are all periodic functions of azimuth angles, $\Theta^B$ and $\Theta^M$, with the same period of $2\pi$. Therefore, we represent them by their FSEs as follows:

TABLE I
REQUIRED NUMBER OF FSCS, $N_{95\%}$, FOR REPRESENTING THE APP WITH 95% OF ITS ENERGY

| Antenna Type | $N_{95\%}$ $h=\frac{c}{4f}$ | $h=\frac{c}{2f}$ | $h=\frac{3c}{4f}$ | $h=\frac{c}{f}$ |
|---|---|---|---|---|
| Half-wavelength dipole | 3 | | | |
| Microstrip antenna | 3 | 3 | 3 | 11 |
| Vertical electric dipole | 7 | 11 | 15 | 19 |
| Finite length dipole | 3 | 3 | 7 | 7 |

$$\mathcal{G}_{p;k}^B \longleftrightarrow G_p^B(\Theta^B;\omega) \quad \text{and}$$
$$\mathcal{G}_{m;k}^M \longleftrightarrow G_m^M(\Theta^M;\omega), \quad (6a)$$
$$\mathcal{G}_k = \frac{1}{2\pi}\int_{-\pi}^{\pi} G(\Theta;\omega)e^{-jk\Theta}d\Theta \quad \text{and}$$
$$G(\Theta;\omega) = \sum_{k=-\infty}^{+\infty}\mathcal{G}_k e^{jk\Theta}. \quad (6b)$$

The APPs of some commonly used antennas in wireless applications are $\Theta \in [-\pi,\pi)$ [15] as shown in (7a) through (7d), where $h$, $h_1$ and $h_2$ are proportional with the size of the antenna and $G_0$ is the positive real constant antenna gain. The half-wavelength dipole and microstrip antenna are often used for antenna arrays [15]. All antennas are assumed to be on the azimuth plane; the axis of dipole antennas are parallel with the azimuth plane. The APPs of the employed antennas at the BS side are normally different from those at the MS side. By numerical simulations, we observe that for these antennas, the value of $|\mathcal{G}_k|$ is only considerable for a limited number of coefficients. We define $N_{95\%}$ as the required number of FSCs that constitute equal or more than 95% of the energy of the APP. Table I, we show $N_{95\%}$ for $h_1 = h_2 \triangleq h$, and $h \in \left\{\frac{c}{4f}, \frac{c}{2f}, \frac{3c}{4f}, \frac{c}{f}\right\}$ and the carrier frequency of $f = \frac{\omega}{2\pi} = 2$GHz. We usually need more coefficients when the size of the antenna increases. One should note that the vertical-electric dipole needs the most number of coefficients to be accurately constructed.

A3) We decompose the $i^{\text{th}}$ path propagation delay, $\tau_{p,m;i}$, into three components: one major delay because of the distance between BS and MS, and two relative propagation delays with respect to local coordinates across BS and MS antenna arrays, as follows:

$$\tau_{p,m;i} = \tau_i - (\tau_{p;i}^B + \tau_{m;i}^M), \quad (8a)$$
$$\tau_{p;i}^B \triangleq \frac{\mathbf{a}_p^{B\,T}\boldsymbol{\Theta}_i^B}{c}, \quad \tau_{m;i}^M \triangleq \frac{\mathbf{a}_m^{M\,T}\boldsymbol{\Theta}_i^M}{c}, \quad (8b)$$

where $(.)^T$ represents the transpose operator, $\tau_i$ represents the delay between $O^B$ and $O^M$, and $\tau_{p;i}^B$ and $\tau_{m;i}^M$ represent relative propagation delays from antenna

$$\text{Half-wavelength dipole:} \quad G(\Theta;\omega) = G_0 j \frac{\cos\left(\frac{\pi}{2}\cos\Theta\right)}{\sin\Theta}, \tag{7a}$$

$$\text{Microstrip antenna:} \quad G(\Theta;\omega) = -G_0 j \frac{\sin\left(\frac{\omega}{2c}h_1\sin\Theta\right)\sin\left(\frac{\omega}{2c}h_2\cos\Theta\right)}{\cos\Theta}, \tag{7b}$$

$$\text{Vertical electric dipole:} \quad G(\Theta;\omega) = G_0 j \sin\Theta\left[2\cos\left(\frac{\omega}{c}h\cos\Theta\right)\right], \tag{7c}$$

$$\text{Finite length dipole:} \quad G(\Theta;\omega) = G_0 j \frac{\cos\left(\frac{\omega}{2c}h\cos\Theta\right)-\cos\left(\frac{\omega}{2c}h\right)}{\sin\Theta}. \tag{7d}$$

elements, $\mathbf{a}_p^B$ or $\mathbf{a}_m^M$, to corresponding coordinates, $O^B$ or $O^M$, respectively [5]. The time-delays $\tau_i$ are assumed to be i.i.d. random variables which are exponentially distributed. Exponential pdf is a common distribution in outdoor propagation environments. The distribution of the time-delay $\tau_i$ is $f_{\tau_i}(x) = \frac{1}{\sigma}e^{-\frac{x-\overline{\tau}+\sigma}{\sigma}}$, $\forall x \geqslant \overline{\tau}-\sigma$, where $\overline{\tau} = E[\tau_i]$ is the mean value to specify the average propagation distance between the MS and the BS, and $\sigma$ is the delay spread.

A4) Assuming $|\tau_i| \gg \max\left\{|\tau_{p;i}^B|, |\tau_{m;i}^M|\right\}$, the path-gain as a function of the time-delay will be:

$$g_{p,m;i} \simeq g_i = \sqrt{\frac{P}{I}}\ {\tau_i}^{-\frac{\eta}{2}}, \tag{9}$$

where $\eta$ is the pathloss exponent and $P$ is a constant. The appropriate value for the pathloss exponent is $\eta = 2$ for free space propagation, $\eta = 4$ for rural and $\eta = 6$ for crowded urban environments [5].

A5) As a consequence of the planar wave propagation, the path phase shift $\phi_i$ accurately approximates $\phi_{p,m;i}$. We take into account the phase contribution of scatterers by uncorrelated random phase changes $\phi_i \sim U[-\pi,\pi)$. See [16], [17] for more complicated and more realistic phase difference models.

## III. Cross-Correlation Function (CCF) for Non-Isotropic Propagation Environments with Directional antennas

The CCF between two sub-channels, $h_{mp}(t_1,\omega_1)$ and $h_{nq}(t_2,\omega_2)$, is defined by,

$$R_{pm,qn}(t_1,t_2;\omega_1,\omega_2) \triangleq E[h_{pm}(t_1,\omega_1)\ h_{qn}^*(t_2,\omega_2)]. \tag{10}$$

Since, this CCF is a function of sampling times $(t_1,t_2)$, carrier frequencies $(\omega_1,\omega_2)$, and antenna elements $(p,m;q,n)$, we call it STF-CCF. By replacing (1) in (10), CCF is written as shown in (11). We decompose the expression of $R_{pm,qn}(t_1,t_2;\omega_1,\omega_2)$ by regrouping dependent and independent variables in (11), replacing $g_i$ from (9), and using Assumptions A1-A4, as shown in (12). For $i_1 = i_2$, the first expectation in (12) is given by [5, Appendix I]:

$$E\left[(\tau_{i_1}\tau_{i_2})^{\frac{-\eta}{2}}\exp\left(j\left(\omega_2\tau_{i_2}-\omega_1\tau_{i_1}\right)\right)\right] = \mathbf{\Phi}_\tau^{(\eta)}\left(j(\omega_2-\omega_1)\right). \tag{13}$$

where $\mathbf{\Phi}_\tau(s) \triangleq \frac{e^{(\mu-\sigma)s}}{1-\sigma s}$ is the moment generating function (MGF) of $\tau$. We also have,

$$E\left[e^{j(\phi_{i_1}-\phi_{i_2})}\right] = \delta_{i_1-i_2}, \tag{14}$$

where $\delta_k$ is the unit impulse. The last two expectations in (12) are calculated in Appendix A. The calculation is proposed for the case $i_1 = i_2$, as the case $i_1 \neq i_2$ results in zero. Hereby, we formulate the CCF as shown in (15a) through (15d). $\mathcal{G}_k(\omega)$ and $\mathcal{F}_k$ are the $k^{\text{th}}$ FSCs of the APP and the AAS in the corresponding coordinates, respectively, $J_k(z) \triangleq \frac{j^{-k}}{\pi}\int_0^\pi e^{j(k\xi+z\cos\xi)}d\xi$ is the $k^{\text{th}}$-order Bessel function of the first kind, $|.|$ denotes Euclidian norm and $z_n \triangleq x_n \otimes y_n = \sum_{k=-\infty}^{+\infty} x_k y_{n-k}$ denotes the linear convolution of two given discrete-time sequences $x_n$ and $y_n$. In Assumption A3, we consider an exponential pdf for the delay profile (DP). By integrating the MGF, $\mathbf{\Phi}_\tau(s)$, $\eta^{\text{th}}$-times, we obtain the expression of $\mathbf{\Phi}_\tau^{(\eta)}(s)$ as given in [5]. The vectors $\mathbf{d}^B$ and $\mathbf{d}^M$ are the separation vectors. These separation vectors illustrate the impact of the location of antennas, the time indices, the carrier frequencies, and the mobile speed on the CCF at BS and MS, respectively. The norm of these vectors (divided by $c$) are the arguments of the Bessel functions. Therefore, these norms represent a combination of the spatial, the temporal, and the frequency separations between $h_{mp}(t_1,\omega_1)$ and $h_{nq}(t_2,\omega_2)$.

For an omnidirectional antenna we have $\mathcal{G}_k = \delta_k$. In this case, the corresponding coefficients $\mathcal{G}_k$ vanishes from the expression of the CCF. Similarly, for an isotropic scattering around either the BS or the MS, we have $\mathcal{F}_k = \frac{1}{2\pi}\delta_k$, i.e., the corresponding coefficients $\mathcal{F}_k$ vanishes from the expression of the CCF. In contrast to the isotropic scattering environment [5], the non-isotropic scattering and the propagation patterns together create the higher order Bessel functions in the expression of the CCF. From (15b), we will show that the coefficients $e^{jk\angle\mathbf{d}}\mathcal{H}_k(\omega)$ are given by the inner product of $\mathcal{W}\left(\mathbf{d},\mathcal{H}_k(\omega)\right)$ with the Chebyshev polynomials in he Fourier domain. In practice by employing only a limited number of Bessel functions in (15a), we obtain an accurate approximation for the CCF, since the APPs and the pdf of the propagation directions are accurately approximated by a limited number of FSCs.

From (15b), we observe that the norm of the separation vectors $|\mathbf{d}|$ appear in the argument of Bessel functions, where its phase modulates the coefficients, i.e., $e^{jk\angle\mathbf{d}}\mathcal{H}_k(\omega)$. This phase modulation plays a significant role on the behavior of the CCF. Obviously, in an isotropic environment and using omnidirectional antennas this phase modulation vanishes.

## IV. Numerical Evaluation of the CCF

We perform different analysis on the derived CCF to see the impact of non-isotropic propagation, directional antennas, and the MS speed on the CCF.

$$R_{pm,qn}(t_1,t_2;\omega_1,\omega_2) = E\Big[\sum_{i_1,i_2=1}^{I} G_p^B(\Theta_{i_1}^B;\omega_1)G_m^M(\Theta_{i_1}^M;\omega_1)g_{p,m;i_1}e^{j(\phi_{i_1}-\phi_{i_2})}e^{-j\omega_1\tau_{p,m;i_1}(t_1)} \times G_q^{B*}(\Theta_{i_2}^B;\omega_2)G_n^{M*}(\Theta_{i_2}^M;\omega_2)g_{q,n;i_2}e^{j\omega_2\tau_{q,n;i_2}(t_2)}\Big] \quad (11)$$

$$R_{pm,qn}(t_1,t_2;\omega_1,\omega_2) = \frac{P}{I}\sum_{i_1,i_2=1}^{I}\Big\{E\left[(\tau_{i_1}\tau_{i_2})^{\frac{-\eta}{2}}e^{j\left(\omega_2\tau_{i_2}-\omega_1\tau_{i_1}\right)}\right]E\left[e^{j(\phi_{i_1}-\phi_{i_2})}\right] \times E\left[G_p^B(\Theta_{i_1}^B;\omega_1)G_q^{B*}(\Theta_{i_2}^B;\omega_2)e^{j\left(\frac{\omega_1}{c}\mathbf{a}_p^{BT}\boldsymbol{\Theta}_{i_1}^B-\frac{\omega_2}{c}\mathbf{a}_q^{BT}\boldsymbol{\Theta}_{i_2}^B\right)}\right] \times E\left[G_m^M(\Theta_{i_1}^M;\omega_1)G_n^{M*}(\Theta_{i_2}^M;\omega_2)e^{j\left(\frac{\omega_1}{c}\left(\mathbf{a}_m^M-\mathbf{v}t_1\right)^T\boldsymbol{\Theta}_{i_1}^B-\frac{\omega_2}{c}\left(\mathbf{a}_n^M-\mathbf{v}t_2\right)^T\boldsymbol{\Theta}_{i_2}^B\right)}\right]\Big\} \quad (12)$$

$$R_{mp,nq}(t_1,t_2;\omega_1,\omega_2) = P\boldsymbol{\Phi}_\tau^{(\eta)}(j(\omega_2-\omega_1))\mathcal{W}\left(\mathbf{d}_{p,q}^B,\mathcal{G}_{p,k}^B(\omega_1)\otimes\mathcal{G}_{q,-k}^{B\ *}(\omega_2)\otimes\mathcal{F}_k^B\right)\times \times \mathcal{W}\left(\mathbf{d}_{m,n}^M,\mathcal{G}_{m,k}^M(\omega_1)\otimes\mathcal{G}_{n,-k}^{M\ *}(\omega_2)\otimes\mathcal{F}_k^M\right) \quad (15a)$$

where,

$$\mathcal{W}(\mathbf{d},\mathcal{H}_k) \triangleq 2\pi\sum_{k=-\infty}^{+\infty} j^k e^{jk\angle\mathbf{d}}\mathcal{H}_k(\omega)J_k(\frac{|\mathbf{d}|}{c}), \quad (15b)$$

$$\mathbf{d}_{p,q}^B \triangleq \omega_1\mathbf{a}_p^B-\omega_2\mathbf{a}_q^B,\quad \mathbf{d}_{m,n}^M \triangleq (\omega_2t_2-\omega_1t_1)\,\mathbf{v}+\left(\omega_1\mathbf{a}_m^M-\omega_2\mathbf{a}_n^M\right), \quad (15c)$$

$$\mathbf{d}_p^B \triangleq \omega_1\mathbf{a}_p^B,\quad \mathbf{d}_q^B \triangleq \omega_2\mathbf{a}_q^B,\quad \mathbf{d}_m^M \triangleq \omega_1(\mathbf{a}_m^M-t_1\mathbf{v}),\quad \mathbf{d}_n^M \triangleq \omega_2(\mathbf{a}_n^M-t_2\mathbf{v}), \quad (15d)$$

### A. Fourier Analysis of the CCF in Stationary Case

We analyze the CCF derived in (15a) in the frequency domain for the stationary case of $\omega_1=\omega_2=\omega$, and $m=n=1$. In this case from $\angle\mathbf{d}_{1,1}^M=\angle\mathbf{v}+\angle(t_2-t_1)$, we get (16). Using (16) and the Fourier transform of $J_k(u)$[1], the Fourier transform of this CCF versus the time-difference index $\Delta t \triangleq t_2-t_1$ results in (17), where $\mathcal{H}_k^B \triangleq \mathcal{G}_{p,k}^B(\omega)\otimes\mathcal{G}_{q,-k}^{B\ *}(\omega)\otimes\mathcal{F}_k^B$. Note that $\mathbf{R}_{p1,q1}(\Lambda,\omega)=0$, for all $|\Lambda|\geqslant\frac{\omega}{c}|\mathbf{v}|$. The Chebyshev polynomials form a complete orthogonal set on the interval $-1\leqslant u\leqslant 1$, with respect to the weighting function $\frac{1}{\sqrt{1-u^2}}$[2]. Therefore, any bandlimited CCF (on the interval $-\frac{\omega}{c}|\mathbf{v}|\leqslant\Lambda\leqslant+\frac{\omega}{c}|\mathbf{v}|$) can be expanded in terms of Chebyshev polynomials as shown in the above expression. The coefficients of this expansion are $\left\{e^{jk\angle\mathbf{v}}\left(\mathcal{G}_{1,k}^M(\omega)\otimes\mathcal{G}_{1,-k}^{M\ *}(\omega)\otimes\mathcal{F}_k^M\right)\right\}$. These coefficients are also obtained by the inner product of the CCF with $T_k(\Lambda)$ (see (17)). In (19), $\mathbf{R}^M(\Lambda)$, is the last term in (17), and represents the impact of the non-isotropic environment, the APP, and the direction of the MS speed, The term, $\mathbf{R}^M(\Lambda)$, is a power spectral density (PSD) that represents the channel variations caused around or by the MS. In Figures 2 this PSD is calculated and depicted for several scenarios that are produced by combinations of:

1) propagation environment: macrocellular ($a=0.2$rad), or microcellular ($a=0.78$rad),
2) distribution of propagation directions around the MS: truncated Normal, truncated Laplace, or the uniform[3] distributions; $\mathcal{F}_k$s are taken from Assumption A1,
3) antenna propagation pattern (commonly used in antenna arrays): omnidirectional, half-wavelength dipole, or microstrip; $\mathcal{G}_k$s are taken from Assumption 2,
4) direction of the MS speed: the positive $x$-axis direction or the positive $y$-axis direction.

Therefore, the maximum Doppler shift is $\frac{\omega|\mathbf{v}|}{c}$ (i.e., $\mathbf{R}^M(\Lambda)=0$ if $|\Lambda|\geqslant\frac{\omega|\mathbf{v}|}{c}$) and the motion direction of the MS has a major effect on the shape of CPS in a non-isotropic environment with directional antenna. For instance in Figures 2a, 2c, and 2e, the CPS is greater at positive $\Lambda$ than at negative $\Lambda$ in average. This is because of the interaction between the beam of the antenna pattern, the direction of the MS movement, and the pdf of the propagation directions. Note that in (19) if we change $\mathbf{v}$ into $-\mathbf{v}$, the CPS changes from $\mathbf{R}^M(\Lambda)$ to $\mathbf{R}^M(-\Lambda)$

[1]We employ the Fourier transform of $J_k(u)$ which is given by,

$$\mathbf{J}_k(\Lambda)\triangleq\mathbf{F}[J_k(u)] = \int_{-\infty}^{+\infty}e^{-j\Lambda\xi}J_k(\xi)d\xi = \begin{cases}\frac{2(-j)^kT_k(\Lambda)}{\sqrt{1-\Lambda^2}}, & \text{if } |\Lambda|<1,\\ 0, & \text{if } |\Lambda|\geqslant 1,\end{cases}$$

where $T_k(\Lambda)\triangleq\cos\left[k\cos^{-1}(\Lambda)\right]$ is the $k^{\text{th}}$-order Chebyshev polynomial function of the first kind.

[2]It can be shown that,

$$\int_{-1}^{1}\frac{1}{\sqrt{1-\xi^2}}T_k(\xi)T_l(\xi)d\xi = \begin{cases}0\,, & k\neq l\,,\\ \pi\,, & k=l=0\,,\\ \frac{\pi}{2}\,, & k=l=1,2,\ldots\end{cases} \quad (18)$$

[3]The isotropic (uniform) scenario is traditionally used in some well-known models such as the Jake's model [1], [18].

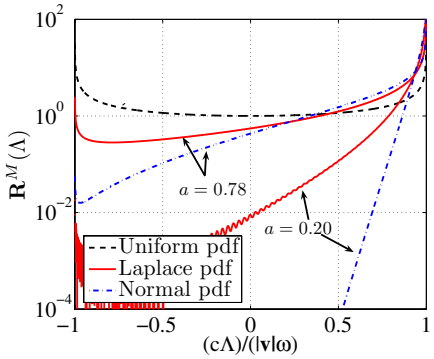


(a) Omnidirectional antenna; moving on the $x$-axis

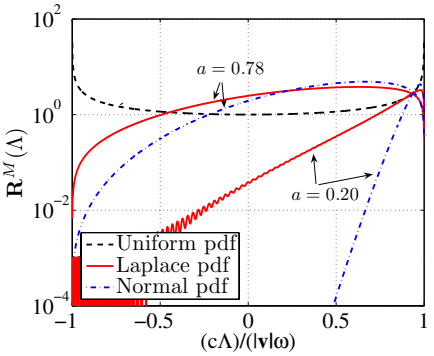


(b) Omnidirectional antenna; moving on the $y$-axis

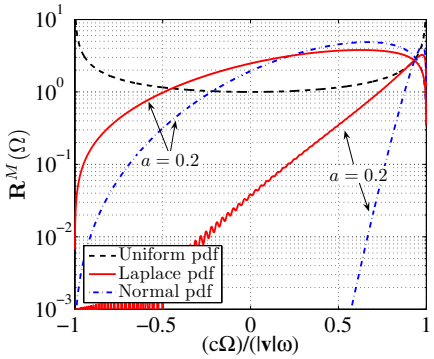


(c) Half-wavelength dipole, moving on the $x$-axis

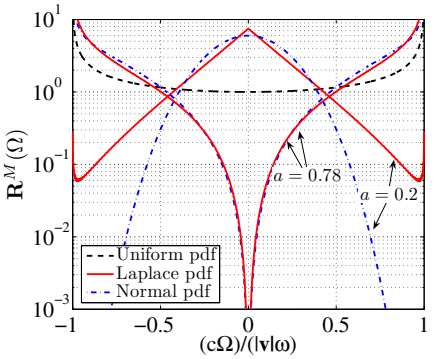


(d) Half-wavelength dipole, moving on the $y$-axis

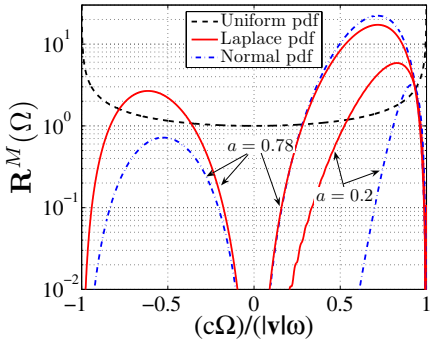


(e) Microstrip antenna, moving on the $x$-axis

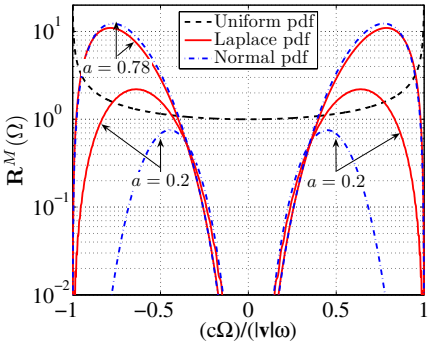


(f) Microstrip antenna, moving on the $y$-axis

Fig. 2. Comparison of Power Spectral Density (PSD): for stationary CCF ($\omega_1 = \omega_2 = \omega$, one antenna at the MS with $h = \frac{c}{2f}$), two non-isotropic (Laplacian and Normally distributed) propagation environments and an isotropic environment (uniformly distributed), two different scenarios of macrocellular ($a = 0.20$rad) and microcellular ($a = 0.78$rad) environments, and three antenna types: Omnidirectional, Half-wavelength dipole, and microstrip antennas. (a), (c), and (e) when MS moves on the positive direction of $x$-axis, (b), (d), and (f) when MS moves on the positive direction of $y$-axis.

$$R_{p1,q1}(t_1,t_2;\omega,\omega) = 2\pi P\mathcal{W}\left(\mathbf{d}^B_{p,q},\mathcal{G}^B_{p,k}(\omega)\otimes\mathcal{G}^{B}_{q,-k}{}^{*}(\omega)\otimes\mathcal{F}^B_k\right)\times \times \sum_{k=-\infty}^{+\infty} j^k e^{jk\angle\mathbf{v}}\left(\mathcal{G}^M_{1,k}(\omega)\otimes\mathcal{G}^{M}_{1,-k}{}^{*}(\omega)\otimes\mathcal{F}^M_k\right) J_k\left(\frac{\omega(t_2-t_1)|\mathbf{v}|}{c}\right). \tag{16}$$

$$\mathbf{R}_{p1,q1}(\Lambda,\omega) \triangleq \int_{-\infty}^{+\infty} e^{-j\Lambda\Delta t} R_{1p,1q}(t_1,t_2;\omega,\omega)d\Delta t = \mathcal{W}\left(\mathbf{d}^B_{p,q},\mathcal{H}^B_k\right) \times\frac{4\pi c}{\omega|\mathbf{v}|}P_0\sum_{k=-\infty}^{+\infty} e^{jk\angle\mathbf{v}}\left(\mathcal{G}^M_{1,k}(\omega)\otimes\mathcal{G}^{M}_{1,-k}{}^{*}(\omega)\otimes\mathcal{F}^M_k\right)\frac{T_k\left(\frac{c}{|\mathbf{v}|\omega}\Lambda\right)}{\sqrt{1-\left(\frac{c}{|\mathbf{v}|\omega}\Lambda\right)^2}}, \quad \text{if } |\Lambda| < \frac{\omega}{c}|\mathbf{v}|, \tag{17}$$

$$\mathbf{R}^M(\Lambda) \triangleq \sum_{k=-\infty}^{+\infty} e^{jk\angle\mathbf{v}} \left(\mathcal{G}^M_{1,k}(\omega) \otimes \mathcal{G}^M_{1,-k}{}^*(\omega) \otimes \mathcal{F}^M_k\right) \frac{T_k\left(\frac{c}{|\mathbf{v}|}\frac{\Lambda}{\omega}\right)}{\sqrt{1-\left(\frac{c}{|\mathbf{v}|}\frac{\Lambda}{\omega}\right)^2}}, \quad |\Lambda| < \frac{\omega}{c}|\mathbf{v}|. \tag{19}$$

(note that $e^{jk\angle\mathbf{v}}$ is the only term that depends on the speed direction). In Figures 2b, 2d, and 2f, all the CPS curves are symmetrical around the axis $\Lambda = 0$. This is because the pdf of the path directions and the APPs are symmetrical around $\Theta^M = 0$, while the MS is moving in a direction perpendicular to them. The CPS for the non-isotropic propagation is deviated from the isotropic U-shaped function [18]. This deviation depends on the antenna pattern (the size and type of employed antenna), the type of the random propagation in the space, as well as the MS speed vector.

If we assume that the speed direction $\angle\mathbf{v}$ in (19) is a random variable independent of all other considered random variables, we can simplify (19) by taking the expectation over $\angle\mathbf{v}$. Thus in this case, if $\mathbf{\Phi}_{\angle\mathbf{v}}(s) = E[e^{s\angle\mathbf{v}}]$ denotes the MGF of $\angle\mathbf{v}$, we get (20).

### B. Fourier Analysis of the CCF in non-Stationary Case

The CCF in (15a) represents a non-stationary process in general. The impact of several parameters are reflected via the separation vectors $\mathbf{d}$. The term $e^{jk\angle\mathbf{d}}$ in (15b) modulates $\mathcal{H}_k$. This phase modulation plays a significant role on the behavior of the CCF. However, the interactions between various parameters is very complicated as is formulated by the CCF in (15a). In order to gain better understanding of these interactions, we can consider the general function $\mathcal{W}(\mathbf{d}, \mathcal{H}_k)$ in (15b) that represents different terms of the derived CCF (15a) when evaluated at different separation vectors $\mathbf{d}$. If we calculate the Fourier transform of $\mathcal{W}(\mathbf{d}, \mathcal{H}_k)$ with respect to the norm of the separation vector $|\mathbf{d}|$ (e.g., either at the BS or at the MS; $\mathbf{d}^B_{p,q}$ or $\mathbf{d}^M_{m,n}$), we obtain similar results as in the above. Therefore, we conclude that the separation effects of the space, time, and carrier frequency are similarly and have duality in their form.

### C. Coherence Time and Coherence Bandwidth

Coherence time (CT), $T_c$, is the separation time over which the fading channel appears to be correlated, while the coherence bandwidth (CB), $B_c$, is the separation between frequencies over which the signal envelope seems to be correlated. Definitions for coherence may be based on the envelope correlation function. A conventional definition for these coherence functions for a SISO communication system is the value of $\Delta$ ($\Delta t = t_2 - t_1 \geqslant 0$ or $\Delta\omega = \omega_2 - \omega_1 \geqslant 0$) which satisfies the equation of the envelope correlation $\rho(\Delta) = 0.5$, where $\rho_{\Delta_t,\Delta_\omega} \triangleq \frac{E[r(t_1;\omega_1)r(t_2;\omega_2)] - E^2[r(t,\omega)]}{E[r^2(t;\omega)] - E^2[r(t,\omega)]}$, $r(t,\omega) \triangleq |h(t,\omega)|$ and $E[r(t,\omega)] = \frac{1}{2}\sqrt{\pi R(t,t;\omega,\omega)}$ [19], [20]. This definition is equivalent to $D_{\Delta t,\Delta\omega} \triangleq \frac{|R(t_1,t_2;\omega_1,\omega_2)|^2}{|R(t_i,t_i;\omega_i,\omega_i)|^2} = 0.5$ (see Appendix B).

Using numerical evaluations, we study the effects of different parameters on the CB and CT under various circumstances.

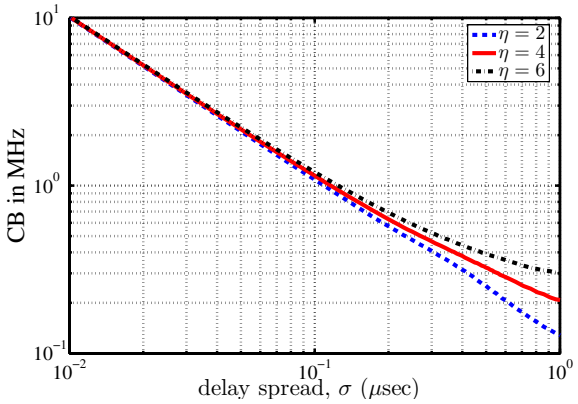


Fig. 3. Coherence bandwidth with respect to the delay spread $\sigma$; using Exponential DP with mean, $\overline{\tau} = 3.33\mu$sec, $t_1 = t_2 = 1$sec, $f_1 = 1$GHz, $|\mathbf{v}| = 60$Km/h, SISO communication system and for different propagation environments with different pathloss exponents $\eta$; free space (typical urban), crowded urban or rural environments with $\eta = 2, 4$, or 6, respectively.

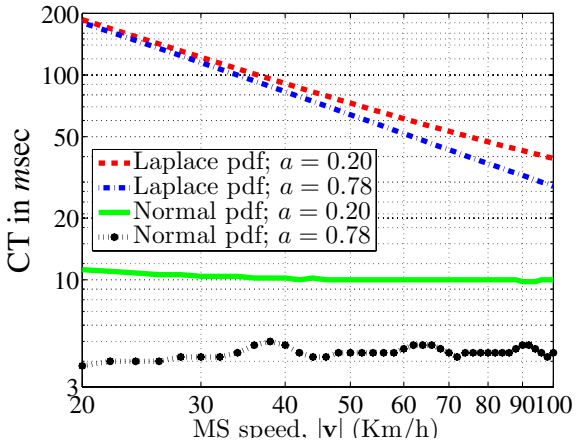


Fig. 4. Average coherence time with omnidirectional antenna, with respect to the value of the MS speed $|\mathbf{v}|$, considering Laplacian and Normally distributed AAS, for two macrocellular ($a = 0.20$rad) and microcellular ($a = 0.78$rad) non-isotropic wave propagation environments; using Exponential DP with $\overline{\tau} = 3.33\mu$sec, $\sigma = 1\mu$sec, $f_1 = f_2 = 2$GHz, $h = \frac{c}{2f}$, and for a SISO communication system.

The CB is defined as $\Delta f\,(\Lambda_{\Delta t,0} = 0.5)$. Our extensive numerical evaluations derived from this model show that in practical situations the CB mostly depends on the delay spread $\sigma$ ($t_1 = t_2 = 1$sec), i.e., it is almost invariant with variations of the parameters of the non-isotropic propagation media, the employed antenna, or the MS speed. In other words, the CB for a narrowband communication system is mostly determined by the delay spread of the DP, $\sigma$. Therefore, consistent with the behavior of wide-sense-stationary uncorrelated-scattering (WSSUS) systems, the proposed CCF in a stationary scenario suggests a WSSUS propagation system for outdoor environments.

$$\mathbf{R}^M(\Lambda) \triangleq \sum_{k=-\infty}^{+\infty} \mathbf{\Phi}_{\angle \mathbf{v}}(jk) \left( \mathcal{G}_{1,k}^M(\omega) \otimes \mathcal{G}_{1,-k}^{M\ *}(\omega) \otimes \mathcal{F}_k^M \right) \frac{T_k\left(\frac{c\,\Lambda}{|\mathbf{v}|\omega}\right)}{\sqrt{1-\left(\frac{c\,\Lambda}{|\mathbf{v}|\omega}\right)^2}}, \quad \text{if } |\Lambda| < \frac{\omega}{c}|\mathbf{v}| \tag{20}$$

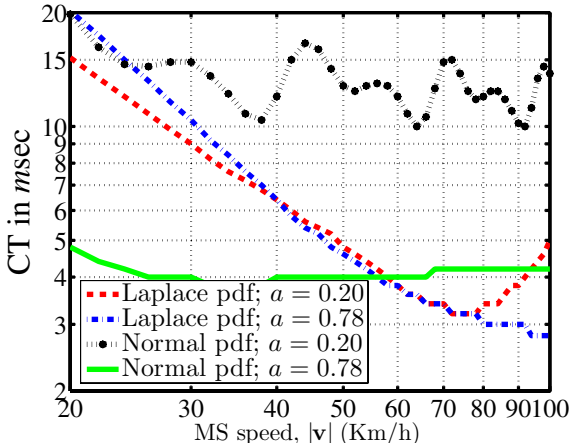


Fig. 5. Average coherence time with half-wavelength antenna, with respect to the value of the MS speed $|\mathbf{v}|$, considering Laplacian and Normally distributed AAS, for two macrocellular ($a = 0.20$rad) and microcellular ($a = 0.78$rad) non-isotropic wave propagation environments; using Exponential DP with $\overline{\tau} = 3.33\mu$sec, $\sigma = 1\mu$sec, $f_1 = f_2 = 2$GHz, $h = \frac{c}{2f}$, and for a SISO communication system.

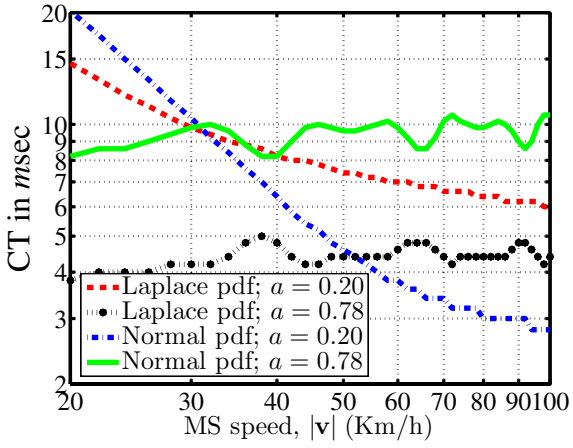


Fig. 6. Average coherence time with microstrip antenna, with respect to the value of the MS speed $|\mathbf{v}|$, considering Laplacian and Normally distributed AAS, for two macrocellular ($a = 0.20$rad) and microcellular ($a = 0.78$rad) non-isotropic wave propagation environments; using Exponential DP with $\overline{\tau} = 3.33\mu$sec, $\sigma = 1\mu$sec, $f_1 = f_2 = 2$GHz, $h = \frac{c}{2f}$, and for a SISO communication system.

Figure 4 shows the CB with respect to $\sigma$ for a typical urban environment ($\eta = 2$), for crowded urban environment ($\eta = 4$), and for rural environment ($\eta = 6$). These values for the CB are close to the average of reported experimental measurements in the literature [21], [22]. The reported values in the literature are between 11.5MHz to 1.2MHz [22] for delay spread values of $0.1\mu$sec to $2\mu$sec [21] in outdoor propagation environments. It turns out that, the CB values reported in the literature under various conditions are accurately predicted using the proposed model. For example, when $|R| = 0.5$, Rappaport in [1] reported an approximation formula for the CB as $\mathrm{CB} \approx \frac{1}{5\sigma}$. This formula results in $\mathrm{CB} = 0.2$MHz for $\sigma = 1\mu$sec which is very close to what is predicted by (21). In order to suggest more accurate formulas for the CB in outdoor environments, Figure 3 illustrates an almost linear relation between the CB and the time-delay delay spread $\sigma$ in a log-log scale, i.e., using a simple curve fitting, we have:

$$\mathrm{CB} \approx k_1 \sigma^{k_2}, \begin{cases} k_1 = 8.9450, & k_2 = -0.7432; \quad \eta = 2, \\ k_1 = 81.4346, & k_2 = -0.6088; \quad \eta = 4, \\ k_1 = 351.6372, & k_2 = -0.5212; \quad \eta = 6. \end{cases} \tag{21}$$

The error in this approximation is less than $\pm 0.75$dB in $|R|$, when the delay spread lies in [0.1-1.1)$\mu$sec (the reported range of delay spread for outdoor environments).

The CT in the literature is reported to be mostly a function of the value of the MS speed (or the maximum Doppler shift) [1], [19]. Our numerical investigations also confirms such a claim in some practical situations; however, we also observe that in contrast of the CB, the CT is considerably influenced by other parameters such as the MS speed direction. This result is expected based on the Fourier analysis on the stationary CCF, as the Doppler effect certainly appears as a function of different parameters of the non-isotropic propagation media, parameters of the employed antenna at the MS side, and the MS speed. The CT is defines as $\Delta t\,(\Lambda_{\Delta t,0} = 0.5)$. In order to evaluate the behavior of the CT, we numerically calculated the CT for different values of the MS speed direction $\angle \mathbf{v}$. Then calculated the average CT over these directions, i.e., $\overline{\mathrm{CT}} \triangleq \frac{1}{2\pi}\int_{-\pi}^{\pi} \mathrm{CT}(\angle \mathbf{v}) d(\angle \mathbf{v})$. This is equivalent to assume that the MS may move in any direction on the azimuthal plane with the same probability. Figures 4, 5, and 6 show the averaged CT with respect the MS speed, $|\mathbf{v}|$ in a log-log scale for three different antennas employed at the MS side; omnidirectional antenna, half-wavelength dipole, and microstrip antenna, respectively. These graphs suggest an almost linear relation between the value of the MS speed and the average CT in a log-log scale for Laplacian distribution. On the other hand for a Normally distributed environment, the average CT is almost constant for all the values of the MS speed. Non-omnidirectional antennas such as the half-wavelength antenna or the microstrip antenna introduce more fluctuations in the graph of the average CT versus $|\mathbf{v}|$. This is because a directional antenna introduces spatial selectivity which interacts with the direction of the MS speed and results in the fluctuations on the Doppler frequency shift and hence on the average CT graph. We note that the CT is invariant with the path-loss exponent and the delay profile as these parameters only appears in the frequency correlation term, $\mathbf{\Phi}_{\tau}^{(\eta)}(j(\omega_2 - \omega_1))$, in (15a) [5]. The average CT results are consistent with the available approximation formulas for the average CT in the literature. For example, when $|R| = 0.5$, Rappaport in [1] gives an approximation formula for the

CT as CT$\approx \frac{9c}{8|\mathbf{v}|\omega}$, where $c$ is the speed of light and $\omega$ is the carrier frequency. Given $|\mathbf{v}| = 60$Km/h and $\omega = 2\pi f$ with $f = 2$GHz, this formula results in CT$= 16.11m$sec which is very close to what is obtained from our model in a macrocellular normal distribution employing omnidirectional antenna. In order to suggest more accurate formulas for the average CT in outdoor environments, we use the same curve-fitting technique being employed for the CB as in [5]. This way, we find the following approximation between the $\overline{\text{CT}}$ and $|\mathbf{v}|$ for the Laplacian distributed environment:

Omnidirectional antenna:

$$\text{CT} \approx k_1|\mathbf{v}|^{k_2}, \begin{cases} k_1 = 6.5839, & k_2 = -0.9219; \quad a = 0.20, \\ k_1 = 7.8541, & k_2 = -1.0641; \quad a = 0.78, \end{cases} \tag{22a}$$

Half-wavelength dipole:

$$\text{CT} \approx k_1|\mathbf{v}|^{k_2}, \begin{cases} k_1 = 1.0750, & k_2 = -1.2223; \quad a = 0.20, \\ k_1 = 2.1396, & k_2 = -1.3979; \quad a = 0.78. \end{cases} \tag{22b}$$

## V. Conclusions

We have calculated the CCF for a MIMO multicarrier channel in a 2D outdoor environment. The contribution in this 2D-CCF model is that this model:

- A1) considers the impact of non-isotropic wave propagation along with directional antenna element patterns,
- A2) accurately takes into account the noticeable effect of the direction and the value of the MS speed,
- A3) gives an accurate expression for the CCF allowing us to analyze the CCF in the frequency domain,
- A4) and gives mathematical expressions to evaluate wireless channels, e.g., developing simulators, calculating approximate expressions for the CB and the CT.

Using a non-geometry approach following [5], the non-isotropic environment and the antenna pasterns are described by their Fourier series expansions. The proposed CCF turns out to be multiplication of three correlation function. The first function is characterized by the parameters of the antennas at the BS and the scatterers around the BS. Similarly, the second function is characterized around the MS. The last correlation function describes the impact of the delay profile and the pathloss component (see [5] for more details about this term). The first two CCFs (in each station) appear as a linear series expansion of averaged Bessel functions of the first kind. The coefficients of this expansion are given by the linear convolution of the FSCs of the corresponding element patterns with the FSCs of the non-isotropic distributions of the angles of scatterers. In practice, this expansion has a limited number of components since the coefficients rapidly converge to zero. The Fourier analysis of the CCF in a stationary case reveals the fact that the channel power spectrum deviates from the U-shaped function (i.e., Jake's/Clark model) to a great extent. This deviation depends on the pdf of the AAS, the employed antennas and the direction of the MS speed. Using the orthogonality between Chebycshev polynomials, we observe that the series expansion coefficients of the Fourier transform of each term of the CCF are also given by the inner product of a Chebycshev polynomial and the Fourier transform of the corresponding term. The expressions for the coherence bandwidth (CB) and the coherence time (CT) are derived and numerically evaluated using the proposed CCF.

Our investigations show that the CB is almost-only a function of the delay spread $\sigma$, while the CT is not only a function of the MS speed (both its value and direction), but also is a function of FSCs representing the non-isotropic propagation medium and the employed antenna. Using these expressions for the CB and CT, we suggest approximation formulas for the CB and CT in different situations.

## Appendix A
## Calculation of the Cross-Correlation Function

This appendix provides details on the calculation of last two expectations in (12), as shown in the equations at the top of the next page. Assuming that $i_1 = i_2 = i$ and using the Fourier series expansions for both APPs and AASs, we are able to calculate these expectations either at the BS or at the MS. As an example, we evaluate this expression at the MS with antennas $m$ and $n$ in (23), where $\mathbf{d}_{m,n}^M \triangleq (\omega_2 t_2 - \omega_1 t_1)\,\mathbf{v} + \left(\omega_1 \mathbf{a}_m^M - \omega_2 \mathbf{a}_n^M\right)$, $\Theta_i^M \triangleq \angle \mathbf{\Theta}_i^M$ and $\mathcal{G}_{m,k}^M(\omega)$, $\mathcal{G}_{n,k}^M(\omega)$, and $\mathcal{F}_k^M$ are the FSCs of the APPs and the AAS in the corresponding coordinates, respectively. $J_k(u) \triangleq \frac{j^{-k}}{\pi}\int_0^\pi e^{ju\cos\xi}\cos(k\xi)d\xi$ is the $k^{\text{th}}$-order Bessel function of the first kind, and $\otimes$ and $|.|$ denote linear convolution and Euclidian norm, respectively. The terms including some time-dependencies appear in the definition of the operand of Bessel functions. This is, of course, in the condition when the direction and the amplitude of the speed of the MS $\mathbf{v}$, are constants. The same calculation procedure is valid for the BS side.

One should note that $\mathcal{G}_{m,k}^M(\omega)$ or $\mathcal{G}_{n,k}^M(\omega)$ absolutely depend on the characteristics of the APPs, $G_m^M(\Theta^M;\omega)$ or $G_n^M(\Theta^M;\omega)$. The APP is usually a well-behaved function, except for the cases when the antenna has a very selective response to a certain direction in the space [15]. For more information on the APPs, see Section II and [15].

## Appendix B
## The Relationship between the CCF and Coherence Time/Coherence Bandwidth

For the envelope process $r(t;\omega)$ in the presence of enough number of multipath waves (where $I$ is large enough), and for $i = 1$ or $i = 2$, we have (24) [19, Pages 47-51] [23], where $\mathcal{E}(.)$ is the complete Elliptic integral of the second kind and $D_{\Delta t,\Delta\omega} \triangleq \frac{|R(t_1,t_2;\omega_1,\omega_2)|^2}{|R(t_i,t_i;\omega_i,\omega_i)|^2}$. We approximate this equation using the expansion of the hypergeometric function [19, Page 51], and obtain:

$$E\left[r(t_1;\omega_1)r(t_2;\omega_2)\right] \approx \frac{\pi}{4}|R(t_i,t_i;\omega_i,\omega_i)|\left(1+\frac{D_{\Delta t,\Delta\omega}}{4}\right). \tag{25}$$

From the above, we get $\rho_{\Delta t,\Delta\omega} = D_{\Delta t,\Delta\omega} = 0.5$. Therefore, using the expression of the CCFs in this dissertations, the CB and the CT are given by the solution of the following equations, respectively, for $\Delta\omega$ and $\Delta t$:

$$D_{0,\Delta\omega} = 0.5, \tag{26a}$$

$$D_{\Delta t,0} = 0.5. \tag{26b}$$

$$E\left[G_p^B(\Theta_{i_1}^B;\omega_1)G_q^{B*}(\Theta_{i_2}^B;\omega_2)e^{j\left(\frac{\omega_1}{c}\mathbf{a}_p^{BT}\mathbf{\Theta}_{i_1}^B-\frac{\omega_2}{c}\mathbf{a}_q^{BT}\mathbf{\Theta}_{i_2}^B\right)}\right]$$

and

$$E\left[G_m^M(\Theta_{i_1}^M;\omega_1)G_n^{M*}(\Theta_{i_2}^M;\omega_2)e^{j\left(\frac{\omega_1}{c}\left(\mathbf{a}_m^M-\mathbf{v}t_1\right)^T\mathbf{\Theta}_{i_1}^M-\frac{\omega_2}{c}\left(\mathbf{a}_n^M-\mathbf{v}t_2\right)^T\mathbf{\Theta}_{i_2}^M\right)}\right].$$

---

$$\begin{aligned}
&E\left[G_m^M(\Theta_i^M;\omega_1)G_n^{M*}(\Theta_i^M;\omega_2)e^{j\left(\frac{\omega_1}{c}\left(\mathbf{a}_m^M-\mathbf{v}t_1\right)^T\mathbf{\Theta}_i^M-\frac{\omega_2}{c}\left(\mathbf{a}_n^M-\mathbf{v}t_2\right)^T\mathbf{\Theta}_i^M\right)}\right]=\\
&=\int_{-\pi}^{\pi}G_m^M(\Theta_i^M;\omega_1)G_n^{M*}(\Theta_i^M;\omega_2)e^{\frac{j}{c}\left(\mathbf{d}_{m,n}^M\right)^T\mathbf{\Theta}_i^M}f_{\mathbf{\Theta}^M}(\Theta_i^M)d\Theta_i^M \qquad (23)\\
&=\int_{-\pi}^{\pi}\sum_{k=-\infty}^{+\infty}\left(\mathcal{G}_{m,k}^M(\omega_1)\otimes\mathcal{G}_{n,k}^{M\ *}(\omega_2)\otimes\mathcal{F}_k^M\right)e^{jk\Theta_i^M+j\frac{\left|\mathbf{d}_{m,n}^M\right|\cos\left(\Theta_i^M-\angle\mathbf{d}_{m,n}^M\right)}{c}}d\Theta_i^M\\
&=2\pi\sum_{k=-\infty}^{+\infty}j^ke^{jk\angle\mathbf{d}_{m,n}^M}\left(\mathcal{G}_{m,k}^M(\omega_1)\otimes\mathcal{G}_{n,-k}^{M\ *}(\omega_2)\otimes\mathcal{F}_k^M\right)J_k\left(|\mathbf{d}_{m,n}^M|/c\right),
\end{aligned}$$

$$E\left[r(t_1;\omega_1)r(t_2;\omega_2)\right]=\frac{1}{2}|R(t_i,t_i;\omega_i,\omega_i)|\left(1+\sqrt{D_{\Delta t,\Delta\omega}}\right)\mathcal{E}\left(\frac{2\sqrt[4]{D_{\Delta t,\Delta\omega}}}{1+\sqrt{D_{\Delta t,\Delta\omega}}}\right), \qquad (24)$$

From (26) we observe that the CB and the CT are functions of various parameters such as the APP of the employed antenna at the MS, AAS of the propagation environment on the MS side, and the speed of the MS.

## REFERENCES


[1] T. S. Rappaport, *Wireless Communications–Principles and Practice*. Prentice Hall PTR, 1996.

[2] D. S. Shiu, G. J. Foschini, M. J. Gans, and J. M. Kahn, "Fading correlation and its effect on the capacity of multielement antenna systems," *IEEE Trans. Commun.*, vol. 48, pp. 502–513, Mar. 2000.

[3] D. Gesbert, H. Bolcskei, D. Gore, and A. Paulraj, "Outdoor mimo wireless channels: models and performance prediction," *IEEE Trans. Commun.*, vol. 50, pp. 1926–1934, Dec. 2002.

[4] A. Abdi and M. Kaveh, "A space–time correlation model for multielement antenna systems in mobile fading channels," *IEEE J. Select. Areas Commun.*, vol. 20, pp. 550–560, Apr. 2002.

[5] S. Gazor and H. S. Rad, "Space-time-frequency characterization of MIMO wireless channels," *IEEE Trans. Wireless Commun.*, to appear.

[6] U. Martin, "Spatio-temporal radio channel characteristics in urban macrocells," *IEE Proc. - Radar, Sonar and Navigation*, vol. 45, pp. 42–49, Feb. 1998.

[7] K. I. Pedersen, P. E. Mogensen, and B. H. Fleury, "A stochastic model of the temporal and azimuthal dispersion seen at the base station in outdoor propagation environments," *IEEE Trans. Veh. Technol.*, vol. 49, pp. 437–447, Mar. 2000.

[8] A. Abdi, J. A. Barger, and M. Kaveh, "A parametric model for the distribution of the angle of arrival and the associated correlation function and power spectrum at the mobile station," *IEEE Trans. Veh. Technol.*, vol. 51, pp. 425–434, May 2002.

[9] S. A. Zekavat and C. R. Nassar, "Power-azimuth-spectrum modeling for antenna array systems: a geometric-based approach," *IEEE Trans. Antennas Propag.*, vol. 51, pp. 3292–3294, Dec. 2003.

[10] A. Tang and K. Gong, "Study on power azimuth spectrum of wireless channel in microcell environments," in *Proc. IEEE Personal, Indoor and Mobile Radio Communications, (PIMRC'03)*, Sept. 2003.

[11] Y. Z. Mohasseb and M. P. Fitz, "A 3d spatio-temporal simulation model for wireless channels," in *Proc. IEEE International Conference on Communications*, vol. 6, pp. 1711–1717, June 2001.

[12] T. D. Abhayapala, T. S. Pollock, and R. A. Kennedy, "Characterization of 3d spatial wireless channels," in *Proc. 58th IEEE Conference on Vehicular Technology*, vol. 1, Orlando, Florida, pp. 123–127, Fall 2003.

[13] Q. Yao and M. Patzold, "Spatial-temporal characteristics of a half-spheroid model and its corresponding simulation model," in *Proc. 59th IEEE Conference on Vehicular Technology*, Milan, Italy, Spring 2004.

[14] H. S. Rad and S. Gazor, "Space-time-frequency characterization of 3d non-isotropic mimo multicarrier propagation channels employing directional antennas," *IEEE Trans. Wireless Commun.*, accepted for publication.

[15] C. A. Balanis, *Antenna Theory: Analysis and Design*. John Wiley & Sons, 2nd ed., 1996.

[16] H. Hashemi, "The indoor radio propagation channel," *Proc. IEEE*, vol. 81, no. 7, pp. 943–968, 1993.

[17] H. Nikookar and H. Hashemi, "Phase modeling of indoor radio propagation channels," *IEEE Trans. Veh. Technol.*, vol. 49, pp. 594–606, Mar. 2000.

[18] R. H. Clarke, "A statistical theory of mobile radio reception," *Bell Syst. Techn. J.*, no. 47, pp. 957–1000, 1968.

[19] W. C. Jakes, *Microware Mobile Communications*. New York: Wiley, 1974.

[20] G. D. Durgin and T. S. Rappaport, "Theory of multipath shape factors for small-scale fading wireless channels," *IEEE Trans. Antennas Propag.*, vol. 48, pp. 682–693, May 2000.

[21] A. Algans, K. Pedersen, and P. Mogensen, "Experimental analysis of the joint statistical properties of azimuth spread, delay spread, and shadow fading," *IEEE J. Select. Areas Commun.*, vol. 20, pp. 523–531, Apr. 2002.

[22] Z. Xiongwen, J. Kivinen, P. Vainikainen, and K. Skog, "Propagation characteristics for wideband outdoor mobile communications at 5.3 ghz," *IEEE J. Select. Areas Commun.*, vol. 20, pp. 507–514, Apr. 2002.

[23] H. Rad and S. Gazor, "A cross-correlation model for non-isotropic scattering with non-omnidirectional antennas in mimo propagation channels," in *Proc. 2005 IEEE 6th Workshop on Signal Processing Advances in Wireless Communications*, pp. 251–255, 2005.

**Hamidreza Saligheh Rad** is born in 1975, Tehran, Iran. He received his B.S. degree from the Electrical Engineering department at Sharif University of Technology (SUT), Tehran, Iran in May 1997; his M.S. degree from the department of Electrical and Computer Engineering at Isfahan University of Technology (IUT), Isfahan, Iran in August 2000. In December 2005, he received Ph.D. in communication engineering from the department of Electrical and Computer Engineering at Queens University and under the supervision of Prof. Saeed Gazor. In January 2006, Hamidreza joined Harvard BroadBand Communications Laboratory (HBBCL) at Harvard School of Engineering and Applied Sciences as a visiting research scholar to be working with Prof. Vahid Tarokh.

Hamidreza has worked in different research areas with his Ph.D. thesis on "Modeling and Evaluation of Wireless Communication Channels," At Harvard, Hamidreza has worked on a number of research problems including "design of frequency-selective pulses for cardiovascular magnetic resonance imaging (MRI)," "advanced communication and networking techniques for satellite communications," and "methods for non-linear three-dimensional inverse imaging."

**Saeed Gazor** (S'94-M'95-SM'98) received the B.Sc. degree in electronics and the M.Sc. degree in communication systems from Isfahan University of Technology, Isfahan, Iran, in 1987 and 1989, respectively, both with the highest standing, and the Ph.D. degree (with highest honors) in signal and image processing from Departement Signal, Telecom Paris, Ecole Nationale Suprieure des Tl-communications/ENST, Paris, France, in 1994.

From 1995 to 1998, he was with the Department of Electrical and Computer Engineering, Isfahan University of Technology. From January 1999 to July 1999, he was with the Department of Electrical and Computer Engineering, University of Toronto, Toronto, ON, Canada. Since 1999, he has been on the Faculty at Queen's University at Kingston, ON, Canada, where he currently holds the position of Associate Professor in the Department of Electrical and Computer Engineering. He is also cross-appointed to the Department of Mathematics and Statistics at Queen's University. His main research interests are array signal processing, statistical and adaptive signal processing, speech processing, MIMO communication systems, networking, analog adaptive circuits, channel modeling, and information theory.

Dr. Gazor received a number of awards, including a Provincial Premier's Research Excellence Award, a Canadian Foundation of Innovation Award, and an Ontario Innovation Trust Award.